RESEARCH ARTICLE | JUNE 17 2025

Quantum transport in the presence of a chiral molecular potential

Ragheed Alhyder ; Mikhail Lemeshko ; Alberto Cappellaro

J. Chem. Phys. 162, 234106 (2025)
https://doi.org/10.1063/5.0271155

The Journal of Chemical Physics ARTICLE pubs.aip.org/aip/jcp

Quantum transport in the presence of a chiral molecular potential

Cite as: J. Chem. Phys. 162, 234106 (2025); doi: 10.1063/5.0271155
Submitted: 15 March 2025 • Accepted: 24 May 2025 •
Published Online: 17 June 2025

Ragheed Alhyder,[1,a)] Mikhail Lemeshko,[1] and Alberto Cappellaro[1,2,3,b)]

AFFILIATIONS

[1] Institute of Science and Technology Austria (ISTA), Am Campus 1, 3400 Klosterneuburg, Austria
[2] Department of Physics and Astronomy "G. Galilei," University of Padova, Via Marzolo 8, 35131 Padova, Italy
[3] National Institute of Nuclear Physics (INFN), Padova Section, Via Marzolo 8, 35131 Padova, Italy

[a)] **Electronic mail:** ragheed.alhyder@ist.ac.at
[b)] **Author to whom correspondence should be addressed:** alberto.cappellaro@unipd.it

ABSTRACT

We investigate quantum transport in a two-dimensional electron system coupled to a chiral molecular potential, demonstrating how molecular chirality and orientation affect charge and spin transport properties. We propose a minimal model for realizing true chiral symmetry breaking on a magnetized surface, with a crucial role played by the tilt angle of the molecular dipole with respect to the surface. For non-zero tilting, we show that the Hall response exhibits clear signatures of chirality-induced effects, in both charge- and spin-resolved observables. Concerning the former, tilted enantiomers produce asymmetric Hall conductances and, even more remarkably, the persistence of this feature in the absence of spin–orbit coupling (SOC) signals how the enantiospecific charge response results from electron scattering off the molecular potential. Concerning spin-resolved observables where SOC plays a relevant role, we reveal that chiral symmetry breaking is crucial in enabling spin-flipping processes.

I. INTRODUCTION AND MOTIVATIONS

In recent years, a significant experimental effort has been made to control the static and transport properties of metallic substrates through the adsorption of chiral molecules on magnetized or superconducting surfaces.[1–6] This highly non-trivial interplay between quantum transport, molecular chirality, and magnetism sits at the core of the so-called Chiral-Induced Spin Selectivity (CISS), an umbrella term encompassing a wide range of phenomena where spin-dependent observables and chiral symmetry breaking are intertwined, spanning open questions from solid-state physics to biochemistry.[7–30]

Investigating chirality in experimental setups is challenging due to the complex interplay between chiral symmetry breaking and intrinsic symmetries of the system's observables. As a result, discerning chirality-driven effects is a non-trivial task, especially on surfaces.[3,31] Indeed, chiral symmetry involves transforming an object into its mirror image, with such pairs called enantiomers. For chiral symmetry breaking to manifest in distinct and measurable effects, enantiomers must result in non-trivial symmetry breaking mechanisms. This is crucial for understanding how chirality affects physical observables, especially for adsorption experiments. There is, indeed, an increasing amount of evidence that surfaces with an out-of-plane magnetization enable an enantiospecific adsorption process,[32] provided that the reaction kinetics occurs on a faster timescale than thermodynamic equilibration. Within the CISS framework, this observation is understood in terms of an emergent spin-exchange interaction arising from the interplay between the magnetized surface and the molecular electric polarizability.[33]

Once this enantiospecific process is established, the main focus of this paper revolves around the resulting chirality-driven signature on transport observables, such as charge- and spin-resolved conductances. By leveraging a minimal model presented in Sec. II, we are able to show that, in a four-terminal setup, enantiospecific signals are present for both charge and spin transport (Sec. III). This occurs in the transverse direction with respect to the injected probe current, a phenomenology reminiscent of the anomalous Hall effect[34] (AHE). Remarkably, the enantiospecificity of the AHE

charge signal appears to be purely driven by electrons scattering off the molecular potential, relating to skew-scattering and side-jump mechanisms[34–37] rather than the intrinsic effects,[38,39] which result from the band structure geometry. As expected, spin–orbit coupling (SOC) becomes increasingly relevant for spin observables. However, we notice that spin-flipping processes are inhibited whenever chiral symmetry is not broken and one can single out a mirror transformation connecting the two enantiomers on the plane. We conclude in Sec. IV by commenting how our results can be possibly framed in terms of the so-called chirality-induced spin selectivity (CISS) and the impact on the development of chirality-enhanced spintronic devices.[11,25]

II. THE MODEL

We examine a minimal theoretical framework able to capture transport properties across a magnetized two-dimensional substrate. We consider the following Hamiltonian for electrons moving in a magnetized substrate:

$$\hat{H}_{\rm tot} = \hat{H}_0 + \hat{H}_{\rm SOC}, \tag{1}$$

where

$$\hat{H}_0 = \frac{\hat{\mathbf{p}}^2}{2m^*} + \Delta\sigma_z + V_{\rm dip}(\mathbf{r}) + V_{\rm ext}(\mathbf{r}). \tag{2}$$

Here, $\hat{\mathbf{p}}$ is the momentum operator of the electron, m^* is the effective mass of the electron, Δ is the exchange field resulting from the magnetized substrate, $V_{\rm ext}$ is the confining potential that defines the scattering region, and $V_{\rm dip}$ is the interaction between electrons and the electric field generated by molecular dipoles.

The molecular potential is modeled as

$$V_{\rm dip}(\mathbf{r}) = e(\boldsymbol{\mathcal{E}}_\mu \cdot \mathbf{r}) \exp\left\{-\frac{\xi_x^2 x^2 + \xi_y^2 y^2 + \xi_z^2 z^2}{2}\right\}, \tag{3}$$

where e is the electron charge, $\boldsymbol{\mathcal{E}}_\mu = 8\boldsymbol{\mu}/\boldsymbol{l}^3$ relates to the electric field proportional to $\boldsymbol{\mu} = (\mu_x, \mu_y, \mu_z)^T$, which acts as the molecular dipole moment, and $\boldsymbol{l}$ is a vector containing the dimensions of the molecule. This form of potential has been used for scattering properties before[40] and is employed here as a model potential to capture the main aspects of the molecular electric field.

The potential in Eq. (3) breaks chiral symmetry. Indeed, a mirror transformation along the x or y axes leads to a rotated potential that is different except for $\mu_x = \mu_y$. Moreover, moving from one enantiomer to the other requires flipping the sign of either μ_x or μ_y. For the sake of simplicity, we keep the sign of μ_x fixed and change μ_y, as the parameter allowing us to switch between both chiralities.

In its current form, the effect of the potential on observables is trivial, since changing the sign of μ_y in Eq. (2) is equivalent to applying a mirror transformation with respect to the xz plane. This leads to any observable having the same value for both enantiomers after applying mirror transformation, as we shall see. This is due to the kinetic term in $\hat{H}_0$ being invariant under mirror symmetry.

To remedy this problem and explore how chiral symmetry-breaking affects the whole Hamiltonian, we consider the possibility of tilting the molecule with respect to the substrate. This is done by introducing an angle θ_w together with the corresponding rotation matrix $\mathscr{R}_{\hat{x}}(\theta_w)$ around the x-axis. Therefore, positions and electric field vectors in Eq. (3) transform into the rotated frame defined as $\mathbf{r}' = \mathscr{R}_{\hat{x}}(\theta_w)\mathbf{r}$, with $\mathbf{r}', \mathbf{r}$ being the coordinate vectors in the lab and molecular frame, respectively. This leads to the following expression:

$$V_{\rm dip}^{LR}(\mathbf{r}) = e\left(\boldsymbol{\mathcal{E}}'_\mu \cdot \mathbf{r}'\right) \exp\left\{-\frac{\xi_x^2 x^2 + \xi_y^2 y'^2 + \xi_z^2 z'^2}{2}\right\}, \tag{4}$$

with

$$\boldsymbol{\mathcal{E}}'_\mu = 8\begin{pmatrix} \mu_x/l_x^3 \\ (\pm\mu_y \cos\theta_w - \mu_z \sin\theta_w)/l_y^3 \\ (\pm\mu_y \sin\theta_w + \mu_z \cos\theta_w)/l_z^3 \end{pmatrix} \tag{5}$$

and $\mathbf{r}' = (x, y\cos\theta_w - z\sin\theta_w, y\sin\theta_w + z\cos\theta_w)$. Different signs of μ_y correspond to the enantiomers. Note that flipping the sign of μ_y here is not equivalent to applying a mirror transformation, providing true chiral symmetry breaking in $\hat{H}_0$, and this point is crucial when considering chirality-dependent effects. Consequently, in the rotated frame, changing the sign of μ_y is sufficient to switching between opposite enantiomers for $\theta_w \neq 0$, without it being equivalent to mirror transformation. We notice here that chirality is actually set by the triple product $\chi = \Delta(\boldsymbol{\mu}_\parallel \times \hat{z}) \cdot \boldsymbol{\mu}_\perp = \Delta\mu_y\mu_z$, involving the out-of-plane substrate magnetization Δ, the in-plane dipole component μ_y, and its out-of-plane counterpart μ_z. A mirror reflection on the $\hat{x} - \hat{z}$ plane flips μ_y and consequently χ, while a rotation around $\hat{z}$ leaves $\mu_y\mu_z$ (and thus χ) unchanged. Hence, chirality remains well defined. Within our model, the potential experienced by electrons on the surface effectively depends on the handedness of the adsorbed molecule only if $\theta_w \neq 0$. If that is not the case, the L- and R-potentials in Eq. (3) are mirror-symmetric. As we show in the following, this implies that, when considering different enantiomers, the response is trivial for $\theta_w = 0$. When the molecule is tilted [i.e., $\theta_w \neq 0$ in Eq. (3)], the charge and spin responses strongly depend on the potential handedness. An analogous scenario is actually observed in the enantiospecific adsorption of chiral molecules upon out-of-plane magnetized surfaces.[32] The enantiospecificity of the molecule–surface interaction is rationalized in terms of an emergent selective spin-exchange interaction and its energetics. More precisely, the substrate is inducing an electric dipole polarization, which in turn is accompanied by a spin polarization whose orientation depends on the molecular chirality.[33] Thus, assuming the presence of this exchange interaction with the magnetized surface, it is possible to extract an effective potential for both enantiomers; according to density-functional calculations,[32] the energy separation between their corresponding minima lies well above the scale of room-temperature fluctuations. It is also important to remark that, as mentioned in the Introduction, in order to observe this enantiospecific process, the reaction timescale has to be shorter than the one related to thermal equilibrium. This feature is strongly dependent from the particular molecular species and experimental conditions, appearing (for now) beyond the grasp of a reliable theoretical modeling.[32] Nevertheless, while we do not claim to reproduce this dynamical and molecule-dependent process, our minimal model actually includes two of the crucial ingredients leading to the above-described enantioselective process, i.e., the molecular electric polarizability and the presence of a magnetic substrate.

As an additional remark, while it is common to distinguish different enantiomers by referring to their handedness (i.e., left vs right), within our framework, this denomination is purely conventional, since these labels do not reflect the geometric structure of the molecule, but rather the different nature of the two potentials is considered.[41] Finally, the field associated with $V_{\rm dip}(\mathbf{r})$ as in Eq. (3) is responsible for the spin–orbit interaction modeled on the Rashba model,[42,43] leading to an additional term defined as

$$\hat{H}_{\rm SOC} = -(\alpha_R/\hbar)\ \boldsymbol{\sigma}\cdot\left[\mathbf{E}_{\rm dip}(\mathbf{r})\times\hat{\mathbf{p}}\right], \tag{6}$$

where $\boldsymbol{\sigma}$ is a vector made of the usual Pauli matrices, $\mathbf{E} = -\nabla V_{\rm dip}(\mathbf{r})$, with $V_{\rm dip}$ being the chiral potential and α_R being the Rashba spin–orbit coupling parameter. Note that all spin-independent observables trace out the SOC contribution, and the discussion above still holds. However, spin-dependent observables will have contributions coming from the SOC, which turn out to be chirality-dependent, as shall be explored in Secs. III A–III C.

Moving to the central issue of chiral symmetry breaking and its signature on transport observables, here we consider a four-terminal device as shown in Fig. 1. This implements a so-called Hall bridge, where $\hat{H}_{\rm tot}$ as in Eq. (1) acts on the central region, specified by blue points in Fig. 1. Four semi-infinite leads are attached to it, acting as electrodes in standard transport experiments. These leads can be thought of as waveguides, driving plane waves in and out of the scattering region. For this reason, the leads Hamiltonian is written as $\hat{H}_L = \mathbf{k}^2/2m^* + \Delta\sigma_z$ in momentum representation such that spin-up/spin-down degeneracy is already lifted.

In order to compute transport observables, we rely upon the scattering wavefunction formalism.[44] While it is completely equivalent to the Keldysh method based on non-equilibrium Green's functions,[45] it is more convenient from a computational perspective and has been implemented in our simulation through the Kwant package.[46,47] This method relies on casting the Hamiltonian $\hat{H}_{\rm tot}$ on a tight-binding discretized model with hopping parameters $t = \hbar^2/(2m^*a^2)$, where a is the lattice constant, Now, considering the four-terminal device displayed in Fig. 1, when a current I_0 is inserted in the left lead, we can measure the (anomalous) Hall response by looking at the voltage drop in the transverse direction, i.e., between the top and bottom leads, as $V_H = V_2 - V_1$. Lead voltages are simply extracted by inverting Ohm's law $\hat{\mathbf{G}}\cdot\mathbf{V} = \mathbf{I}$, where $\hat{\mathbf{G}}$ is the conductance matrix. Its elements G_{ij} represent the conductance between leads i and j ($i \neq j$) as computed by numerically solving the scattering problem. More precisely, for a fixed energy E, we have[44,48,49]

$$G_{ij}(E) = \left(\frac{e^2}{h}\right)\sum_{n\in i}\sum_{n'\in j}|t^{ij}_{nn'}(E)|^2, \tag{7}$$

where n is the index labeling the modes open for conduction at energy E in lead i, and similarly for n', with $t^{ij}_{nn'}(E)$ being the corresponding transmission scattering amplitude. More specifically, these coefficients are the elements of $\hat{\mathbf{t}}^{ij}(E)$, a matrix whose dimension is $\mathcal{N}^i(E)\times\mathcal{N}^j(E)$, with $\mathcal{N}^{i(j)}(E)$ being again the number of open conducting modes in lead $i(j)$. In turn, $\hat{\mathbf{t}}^{ij}(E)$ is an off-diagonal block of the whole scattering matrix $\hat{\mathbf{S}}(E)$ for the N-terminal device.

Except when otherwise specified, the system is solved using experimentally relevant parameters, where we set the effective mass and the lattice constant as $m^* \simeq 0.067m_e$ and $a \simeq 7.1$ Å, respectively; energies are reported in units of the hopping parameter $t = \hbar^2/(2m^*a^2)$, which is readily computed to be around 1.14 eV. As for the Rashba SOC, we set $\alpha_R = 0.1$ eV · Å; corresponding, in our simulations, to $\alpha_R/(2a) \simeq 0.006t$. In order to extract V_H, we apply a current $I_0 = 3\ \mathrm{e}\cdot t/h \simeq 1.0$ mA onto the left lead, with respect to Fig. 1. As mentioned above, spin degeneracy is removed by considering the exchange field coming from the magnetized surface, here $\Delta \simeq 0.001t$. As for the molecular potential $V_{\rm dip}(\mathbf{r})$ in Eq. (3), our values are comparable to the 1,2-propanediol molecule such that $l_x = 2.0$ nm, $l_y = 4.0$ nm, and $l_z = 10$ nm, while the electric dipole components are set to $\mu_x = 2.4$ D, $\mu_y = 5.0$ D, and $\mu_z = 1.8$ D.[50]

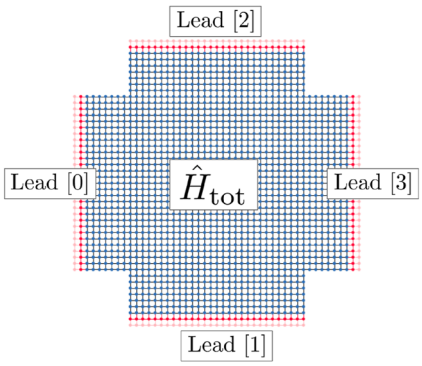

FIG. 1. Instance of a four-terminal Hall setup. The Hamiltonian $\hat{H}_{\rm tot}$, as given by Eq. (1), is implemented in the central (blue) region. Four semi-infinite leads (red) are attached to it. In order to lessen the onset of shape-induced resonances, in the numerical simulations, we actually consider a square-shaped scattering region, whose dimension is 56 × 56 sites.

III. RESULTS

A. Conductance and Hall voltage

First, it is important to explore the dependence of the overall Hall response at different values in such energy and its dependence on SOC strength, as shown in Fig. 2.

We focus on the Hall conductance G_H defined as[48]

$$G_H(E) = \frac{1}{2}\left[G_{20}(E) - G_{10}(E)\right], \tag{8}$$

with the numbering referring to the setup displayed in Fig. 1. In Fig. 2(a), we report the Hall conductance G_H as a function of the Fermi energy ε_F for the whole bandwidth $[-4t-\Delta, 4t+\Delta]$ for different values of the tilting angle θ_w. For every value of θ_w, we plot the results for both handedness values, with solid lines corresponding to $\mu_y > 0$ and dashed lines corresponding to $\mu_y < 0$. It is worth noting that, in practice, we work in the low-temperature limit $T \ll T_F$, with the Fermi energy determining how many lead modes are open for conduction. In order to provide an order of magnitude, for conventional heterostructures where Hall measurements are routinely carried on,[34] the Fermi energy is typically ∼0.2–0.8 eV, corresponding to $T_F \sim 2\cdot 10^3$ K, such that $T/T_F \lesssim 0.15$ at room temperature ($T \sim 300$ K). In this degenerate regime, the zero-temperature Landauer formula holds: taking into account finite-temperature effects

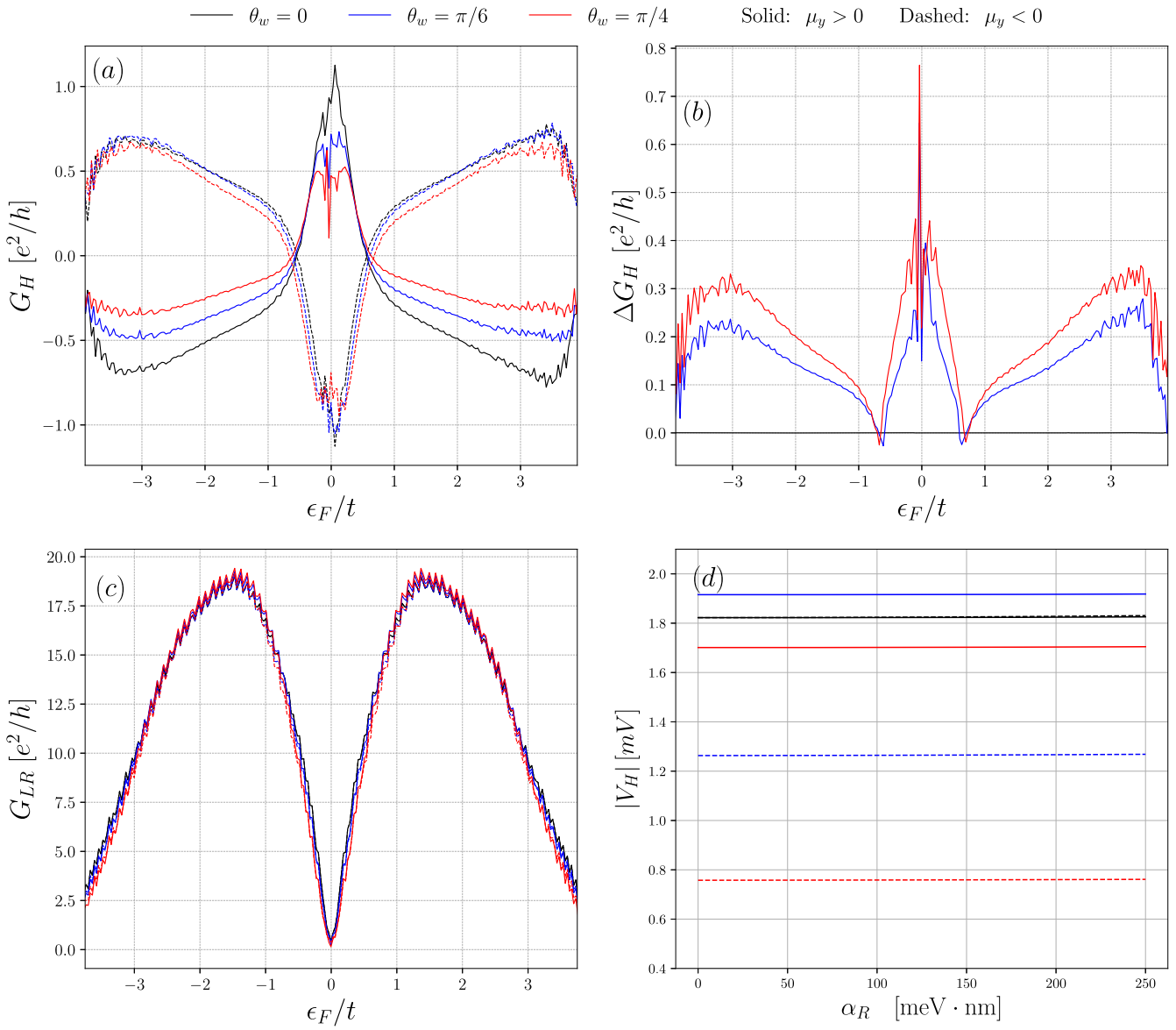

FIG. 2. (a) Hall conductance G_H [defined in Eq. (8)] as a function of the Fermi energy ε_F, here in units of the hopping parameter for the tight-binding model $t = \hbar^2/(2m^* a^2)$. As pointed out in the main text, $\alpha_R/(2a) \simeq 0.006t$ and $\Delta \simeq 0.001t$. We report three different values of the tilting angle θ_w, from $\pi/4$ (red lines) down to $\pi/6$ (blue lines) and 0 (black lines), for both of potential's handedness, with solid lines corresponding to $\mu_y > 0$ and dashed lines corresponding to $\mu_y < 0$. (b) Plot of $\Delta G_H = |G_H^{(L)}| - |G_H^{(R)}|$ as a function of the Fermi energy for the same three values of θ_w listed above. (c) Longitudinal conductance, defined as $G_{LR}(E) = G_{30}(E)$, where the subscripts refer to Fig. 1 lead numbering. As for the above panels, $\theta_w = 0, \pi/6$, and $\pi/4$, but here no difference is observed due to the potential chirality. (d) Absolute value of the Hall voltage V_H at $\varepsilon_f/t \simeq 0.1$ for different values of the spin–orbit coupling constant α_R, while the rest of the simulation parameters are the same as in the previous figures. For the sake of clarity, we just consider the case of $\theta_w = 0$ (no difference between the two enantiomers) and $\theta_w = \pi/4$, where we see a spread of the order ∼1 mV.

would imply convoluting the conductances with the derivatives of the Fermi–Dirac distribution, leaving the crucial features of our model unchanged. Here, we also remark that, within our tight-binding implementation, the tilt is introduced by a rotation $\mathscr{R}_{\hat{x}}(\theta_w)$ [cfr. Eq. (5)] of the molecular dipole. A further azimuthal rotation $\mathscr{R}_{\hat{z}}(\phi)$ around the surface would merely rotate the potential within the scattering region's plane. For ideal, disorder-free leads, this operation leaves the conductance matrix unchanged, since the system possesses full C_∞ in-plane symmetry.

By increasing the electron energy from the left band edge (∼$-4t$), and except for oscillations resulting from the discretizing procedure and the finite system size, the Hall conductance displays a non-monotonic behavior, reaching its maximum as we approach the band center ($\varepsilon_F = 0$), and dropping to zero at the band edges where

no propagating modes remain, so all transmissions vanish and the Hall signal naturally goes to zero. In addition, Fig. 2(a) shows two other zero crossings of the Hall conductance inside the band. These crossings occur when the tilted dipole deflects exactly the same charge to the top and bottom probes: a slight energy shift makes the slowest states pick up an extra phase, flipping their deflection, and cancel the net Hall current. The behavior of the conductance is not considerably affected by the molecular configuration. However, it is immediate to realize that different enantiomers induce responses with opposite sign, a feature observed in a series of seminal experiments with absorbed chiral molecules upon magnetized surfaces.[5]

More remarkably, our framework also adds another crucial detail: depending on the molecular tilting angle θ_w, different enantiomers lead to asymmetric responses (i.e., different absolute values for G_H). For $\theta = 0$, we show that changing handedness is equivalent to taking the mirror transformation counterpart of the conductance, with no change in the amplitude, as discussed before. Meanwhile, for $\theta \neq 0$, the conductance is non-trivially affected by the symmetry breaking introduced in the scattering region by the chiral transformation on the potential. This leads to a relevant difference in the amplitudes of G_H for different enantiomers, as evident by looking at Fig. 2(b), where we plot $\Delta G_H(E) = |G_H^{(L)}| - |G_H^{(R)}|$ for each value of θ_w mentioned above. There, we see that the response is perfectly symmetric if the potential is orthogonal to the magnetized substrate ($\theta_w = 0$), but as soon as the molecule is tilted, a difference between left and right enantiomers emerges. This goes back to the fact that the sign flip in the case of $\theta_w = 0$ is expected, since changing the sign of μ_y is equivalent to applying a mirror transformation along the y-axis in the scattering region of the molecule.

In order to highlight the peculiar behavior of G_H, we also show the longitudinal conductance G_{LR} between leads 0 and 3 in Fig. 2(c). This conductance is equally symmetric with respect to ε_F and reaches a maximum around $\varepsilon_F/t \approx 1$ and vanishes at the edges of the bands as expected.[51] Importantly, we notice how the handedness of the superimposed potential does not influence transport in the longitudinal direction.

Finally, an experimentally relevant observable is the transverse Hall voltage V_H with respect to the spin–orbit coupling, reported in Fig. 2(d). The results of the numerical simulation show a constant value of the Hall voltage V_H (at the fixed value of $\varepsilon_F/t \simeq 0.1$) with respect to the SOC parameter α_R. The Hall voltage only changes signs by moving from one enantiomer to the other one (by flipping the sign of μ_y) when the molecule is not tilted ($\theta_w = 0$). The reason is once again to be found in the transformation leading to the other enantiomer being equivalent to a mirror transformation with respect to the xz plane, flipping in turn the sign of V_H. Therefore, when plotting the absolute value, both enantiomers produce the same values of the Hall voltage.

Meanwhile, for $\theta \neq 0$, we find that the value of the Hall voltage changes as well as its sign. This behavior mimics the one observed experimentally for the anomalous Hall effect when chiral molecules are adsorbed on a two-dimensional metal in Ref. 5, and while the difference in the absolute value of the resistance

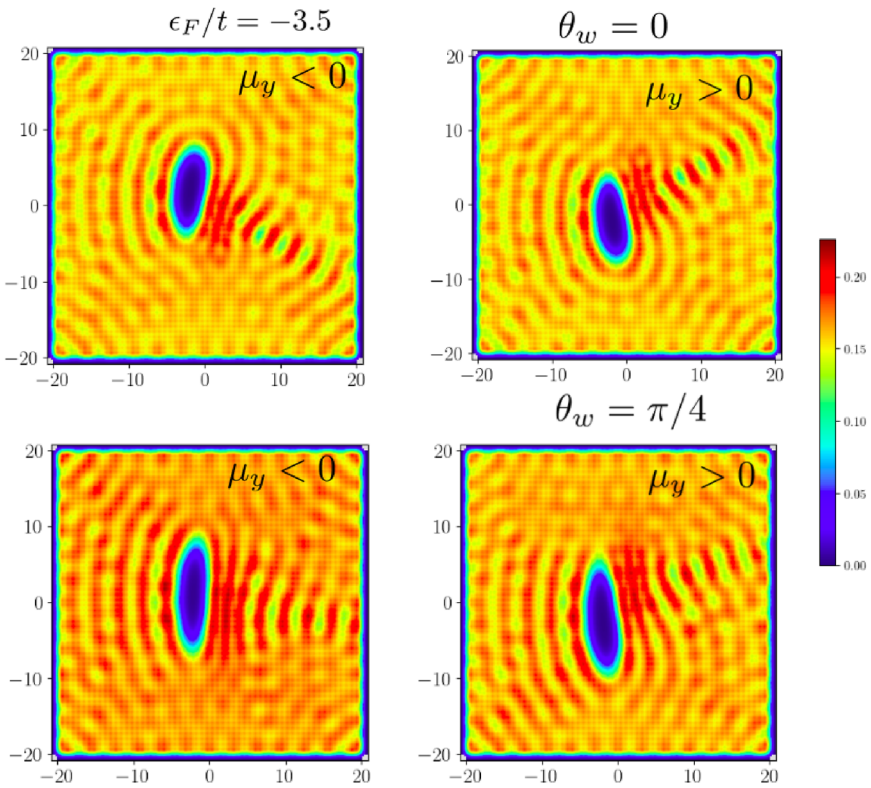

FIG. 3. Local density of states at $E = -3.5t$, as defined in Eq. (9), for both potential handedness ($\mu_y \lessgtr 0$). We consider two tilting angles, $\theta_w = 0$ (top panels) and $\theta_w = \pi/4$ (bottom panels). Similarly to the choice made in Fig. 2, we set $\alpha_R = 0.1$ eV · nm, resulting in $\alpha_R/(2a) \simeq 0.006\,t$ and $\Delta = 0.001\,t$. As discussed in the main text, for $\theta_w = 0$, we can easily identify a mirror plane at $x = 0$, while this is not at all possible when the molecular potential is tilted as in the bottom panels.

was attributed to experimental imperfections, we show that breaking chiral symmetry in the way we outlined can lead to such an effect.

It is also important to notice that we report the same values of the Hall voltage for $\alpha_R = 0$. This leads to the conclusion that the finite value of the voltage is related to electrons scattering off the molecular potential, with no need to include additional forces. This effect can be related to skew-scattering[35] and side-jump[36] contributions to the anomalous Hall conductivity.

B. Density of states

Figure 3 presents the local density of scattering states (LDOS) within our four-terminal device. It is important to distinguish the LDOS from the conventional density of states (DOS), as the LDOS provides spatially resolved information about the distribution of electronic states within the scattering region. Formally, the LDOS is simply defined as

$$\rho(\mathbf{r}, E) = \sum_j |\psi_j^{(S)}(\mathbf{r})|^2 \, \delta(E - \varepsilon_j), \tag{9}$$

where $\psi^{(S)}j(\mathbf{r})$ represents the scattering wavefunction at position $\mathbf{r}$ and ε_j are the corresponding eigenenergies.

Examining the top panels of Fig. 3 for $\theta_w = 0$, we observe that the LDOS remains symmetric with respect to the two potential handedness configurations. This symmetry suggests that, in this particular setup, changing the chirality of the molecule does not induce a significant spatial redistribution of scattering states. The scattering processes in these panels are related by mirror symmetry, consistent with the symmetry of the potential for $\theta_w = 0$.

However, when the molecule is tilted ($\theta_w \neq 0$), as shown in lower left panels, this mirror symmetry is broken. The scattering

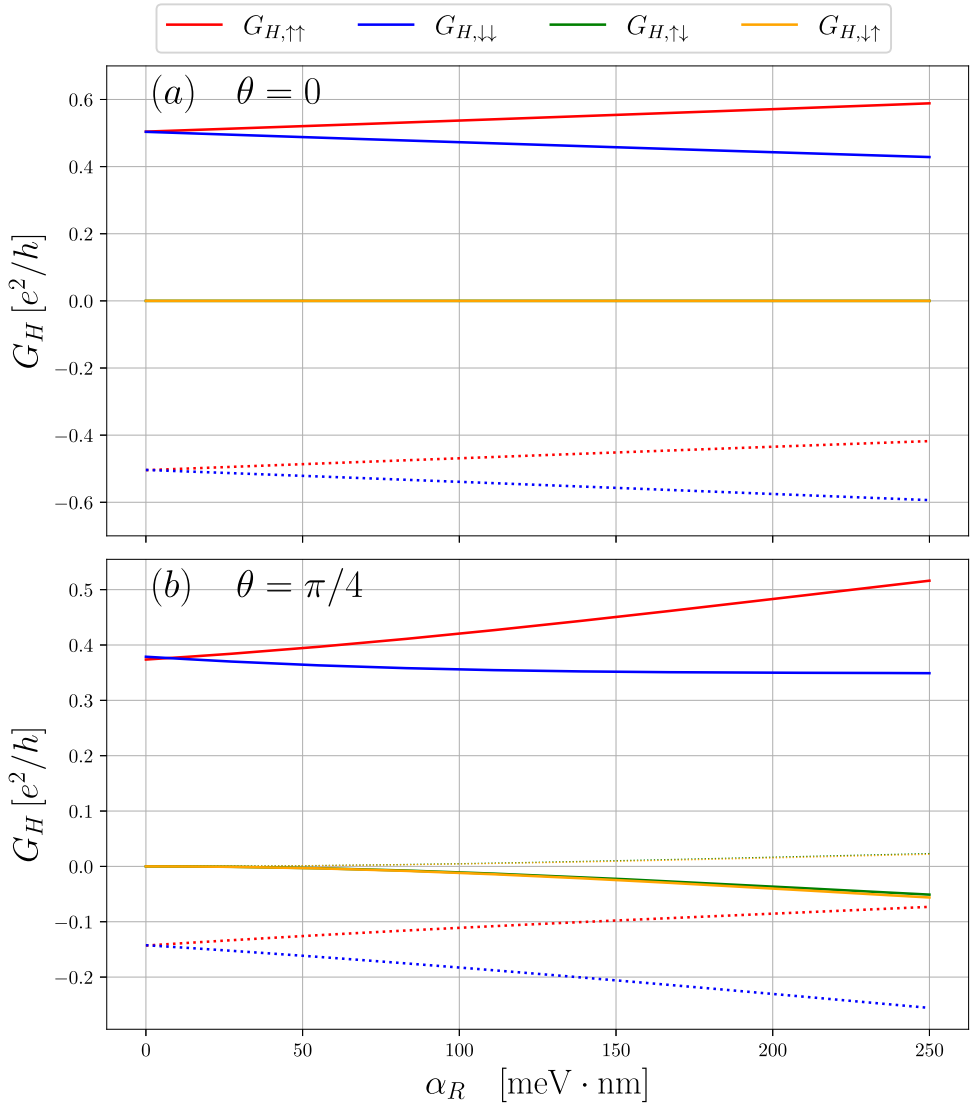

FIG. 4. Spin dependent Hall conductance for different spin components with $\theta = 0$ in panel (a) and $\theta = \pi/4$ in panel (b) as a function of the SOC parameter α_R close to the band center. The solid lines represent $\mu_y > 0$, and the dashed lines represent $\mu_y < 0$. While α_R is increased up to 250 meV · nm, all the other parameters are kept as in Figs. 2 and 3. Once again, we remark the symmetry observed for $\theta_w = 0$ together with the spin-flipping components of the conductance being strictly zero, signaling that these processes are inhibited for this potential mirror-symmetric configuration. This significantly changes when the potential is tilted, as discussed in the main text.

processes in these panels are no longer related by a simple reflection, indicating that the chiral potential asymmetrically influences the spatial distribution of the scattering states. This asymmetry highlights the role of θ_w in determining the symmetry properties of the scattering processes, with the tilted configuration introducing a chiral-dependent modification to the system's electronic behavior.

While the LDOS provides valuable insights into the spatial redistribution of states, it remains spin-independent. To gain a deeper understanding of the role of chirality in spin transport, we now turn to spin-resolved quantities, which reveal critical information about spin-selective effects that cannot be captured by the LDOS alone. These spin-resolved measurements are essential for accurately characterizing chirality-induced transport phenomena, as spin-independent observations may overlook important asymmetries arising from spin-dependent interactions.

C. Spin-dependent transport

To elucidate the importance of chiral symmetry breaking in the problem, we move to spin-dependent observables. The spin-resolved Hall conductance curves shown in Fig. 4 reveal distinct behaviors depending on the orientation angle θ of the chiral molecule relative to the electronic system.

For $\theta = 0$ in Fig. 4(a), the Hall conductance components, $G_{\uparrow\uparrow}$ and $G_{\downarrow\downarrow}$, increase (decrease) linearly, keeping the total conductance constant. In addition, these two components exhibit mirror symmetry. In a consistent manner with the discussion in the spin-independent observables, this symmetry arises from the fact that changing the handedness of the chiral molecule in this configuration is equivalent to applying a mirror transformation, effectively interchanging the spin-up and spin-down components. As a direct consequence, the spin-mixed conductances, $G_{\uparrow\downarrow}$ and $G_{\downarrow\uparrow}$, remain strictly zero, which is consistent with expectations for a system governed by a mirror-symmetric operator. This confirms that, in this regime, spin-flip processes are inhibited, preserving spin coherence in the transport channel.

In contrast, for $\theta = \pi/4$ in Fig. 4(b), the system no longer exhibits mirror symmetry. While the total conductance remains independent of the SOC parameter α_R [cfr. Fig. 2(d)], a notable change occurs in the spin-mixed conductance components $G_{\uparrow\downarrow}$ and $G_{\downarrow\uparrow}$. These values deviate from zero and do not mirror each other, indicating that spin-flip transitions are now allowed. The breaking of mirror symmetry by the chiral potential in this tilted configuration thus modifies the spin-dependent scattering processes, enabling coupling between spin-up and spin-down states.

This is an indication that the symmetry-breaking induced by the chiral molecule's tilted orientation can significantly modify spin-dependent scattering processes, allowing spin-flipping transitions. The observed behavior underscores the critical role of the molecular orientation and chirality in controlling spin transport, highlighting a mechanism through which spin-selective conductance can be engineered. In the context of the ongoing debate within the CISS community, our results in Fig. 4 suggest that the adsorbed molecular structure is actually acting as a spin-polarizer. Indeed, the RSOI enables spin-flipping scattering processes, whose enantiospecificity is evident only when $\theta_w \neq 0$, consistently with our results on charge transport. As previously mentioned, our minimal model cannot reproduce the full picture of the ongoing spin-polarization (and in particular its magnitude[8]). Nevertheless, within a range of reasonable experimental values for α_R, enantiospecific spin-flipping processes are actually contributing significantly to the whole transport picture.

IV. CONCLUSIONS AND FUTURE PERSPECTIVES

We have numerically explored the effects of breaking chiral symmetry on transport properties of a conventional two-dimensional electronic gas. We showed that a significant asymmetry in the hall response arises due to this symmetry breaking. This paves the way for more careful studies of the effects of chiral symmetry breaking on the topological properties of the bands in such a system and how this ties in the picture of CISS.[11,26]

We also showed the importance of chiral symmetry breaking on spin-dependent observables, where chirality, if introduced properly into the system, can introduce spin-flip processes. This behavior highlights the profound impact of the molecular orientation and chirality on spin transport. The ability to selectively break spin symmetry through a controllable parameter introduces a powerful mechanism for engineering spintronic devices. In particular, the observed asymmetry in spin-mixed conductances suggests potential applications in spin-selective filtering and spin-based logic operations, where controlling spin-flip processes is crucial.

Moreover, the persistence of the total conductance's invariance with respect to spin–orbit coupling underscores that the chiral potential primarily affects spin mixing rather than overall charge transport, emphasizing the role of chirality in tailoring spin responses in low-dimensional systems. More importantly, this study highlights the importance of spin-resolved measurements when exploring chiral-induced spin properties.

ACKNOWLEDGMENTS

We thank Artem Volosniev, Narcis Avarvari, Georgios Koutentakis, Sandro Wimberger, and Binghai Yan for useful discussions. R.A. received funding from the Austrian Academy of Science ÖWA, Grant No. PR1029OEAW03. M.L. acknowledges support by the European Research Council (ERC) Starting Grant No. 801770 (ANGULON). A.C. received funding from the European Union's Horizon Europe research and innovation program under the Marie Skłodowska-Curie Grant Agreement No. 101062862-NeqMolRot.

AUTHOR DECLARATIONS

Conflict of Interest

The authors have no conflicts to disclose.

Author Contributions

Ragheed Alhyder: Conceptualization (equal); Data curation (equal); Formal analysis (equal); Funding acquisition (equal); Investigation (equal); Methodology (equal); Project administration (supporting); Resources (supporting); Software (equal); Validation (equal); Visualization (equal); Writing – original draft (equal); Writing – review & editing (equal). **Mikhail Lemeshko**: Conceptualization (equal);

Data curation (equal); Formal analysis (equal); Funding acquisition (equal); Investigation (equal); Methodology (equal); Project administration (lead); Resources (lead); Software (equal); Supervision (lead); Validation (equal); Visualization (equal); Writing – original draft (supporting); Writing – review & editing (equal). **Alberto Cappellaro**: Conceptualization (equal); Data curation (equal); Formal analysis (equal); Funding acquisition (equal); Investigation (equal); Methodology (equal); Project administration (supporting); Resources (supporting); Software (equal); Validation (equal); Visualization (equal); Writing – original draft (equal); Writing – review & editing (equal).

DATA AVAILABILITY

The code to reproduce our results within the scattering wavefunction approach is available upon request, and it is based upon the open source Python package Kwant presented in Ref. 46.

REFERENCES

[1] I. Carmeli, G. Leitus, R. Naaman, S. Reich, and Z. Vager, "Magnetism induced by the organization of self-assembled monolayers," J. Chem. Phys. **118**, 10372–10375 (2003).

[2] Y. Yamamoto, T. Miura, M. Suzuki, N. Kawamura, H. Miyagawa, T. Nakamura, K. Kobayashi, T. Teranishi, and H. Hori, "Direct observation of ferromagnetic spin polarization in gold nanoparticles," Phys. Rev. Lett. **93**, 116801 (2004).

[3] K.-H. Ernst, "Molecular chirality at surfaces," Physica Status Solidi B **249**, 2057–2088 (2012).

[4] O. B. Dor, S. Yochelis, S. P. Mathew, R. Naaman, and Y. Paltiel, "A chiral-based magnetic memory device without a permanent magnet," Nat. Commun. **4**, 2256 (2013).

[5] O. Ben Dor, S. Yochelis, A. Radko, K. Vankayala, E. Capua, A. Capua, S.-H. Yang, L. T. Baczewski, S. S. P. Parkin, R. Naaman, and Y. Paltiel, "Magnetization switching in ferromagnets by adsorbed chiral molecules without current or external magnetic field," Nat. Commun. **8**, 14567 (2017).

[6] H. Alpern, K. Yavilberg, T. Dvir, N. Sukenik, M. Klang, S. Yochelis, H. Cohen, E. Grosfeld, H. Steinberg, Y. Paltiel, and O. Millo, "Magnetic-related states and order parameter induced in a conventional superconductor by nonmagnetic chiral molecules," Nano Lett. **19**, 5167–5175 (2019).

[7] Z. Xie, T. Z. Markus, S. R. Cohen, Z. Vager, R. Gutierrez, and R. Naaman, "Spin specific electron conduction through DNA oligomers," Nano Lett. **11**, 4652–4655 (2011).

[8] R. Gutierrez, E. Díaz, R. Naaman, and G. Cuniberti, "Spin-selective transport through helical molecular systems," Phys. Rev. B **85**, 081404 (2012).

[9] A.-M. Guo and Q.-f. Sun, "Spin-selective transport of electrons in DNA double helix," Phys. Rev. Lett. **108**, 218102 (2012).

[10] A.-M. Guo and Q.-f. Sun, "Sequence-dependent spin-selective tunneling along double-stranded DNA," Phys. Rev. B **86**, 115441 (2012).

[11] R. Naaman and D. H. Waldeck, "Spintronics and chirality: Spin selectivity in electron transport through chiral molecules," Annu. Rev. Phys. Chem. **66**, 263–281 (2015).

[12] S. Varela, V. Mujica, and E. Medina, "Effective spin-orbit couplings in an analytical tight-binding model of DNA: Spin filtering and chiral spin transport," Phys. Rev. B **93**, 155436 (2016).

[13] A. C. Aragonès, E. Medina, M. Ferrer-Huerta, N. Gimeno, M. Teixidó, J. L. Palma, N. Tao, J. M. Ugalde, E. Giralt, I. Díez-Pérez, and V. Mujica, "Measuring the spin-polarization power of a single chiral molecule," Small **13**, 1602519 (2017).

[14] K. M. Alam and S. Pramanik, "Spin filtering with poly-T wrapped single wall carbon nanotubes," Nanoscale **9**, 5155–5163 (2017).

[15] H. Lu, J. Wang, C. Xiao, X. Pan, X. Chen, R. Brunecky, J. J. Berry, K. Zhu, M. C. Beard, and Z. V. Vardeny, "Spin-dependent charge transport through 2D chiral hybrid lead-iodide perovskites," Sci. Adv. **5**, eaay0571 (2019).

[16] M. Atzori and R. Sessoli, "The second quantum revolution: Role and challenges of molecular chemistry," J. Am. Chem. Soc. **141**, 11339–11352 (2019).

[17] R. Naaman, Y. Paltiel, and D. H. Waldeck, "Chiral molecules and the electron spin," Nat. Rev. Chem. **3**, 250 (2019).

[18] M. Geyer, R. Gutierrez, V. Mujica, and G. Cuniberti, "Chirality-induced spin selectivity in a coarse-grained tight-binding model for helicene," J. Phys. Chem. C **123**, 27230–27241 (2019).

[19] X. Yang, C. H. van der Wal, and B. J. van Wees, "Spin-dependent electron transmission model for chiral molecules in mesoscopic devices," Phys. Rev. B **99**, 024418 (2019).

[20] A. Ghazaryan, M. Lemeshko, and A. G. Volosniev, "Filtering spins by scattering from a lattice of point magnets," Commun. Phys. **3**, 178 (2020).

[21] X. Yang, C. H. van der Wal, and B. J. van Wees, "Detecting chirality in two-terminal electronic nanodevices," Nano Lett. **20**, 6148–6154 (2020).

[22] R. Naaman, Y. Paltiel, and D. H. Waldeck, "Chiral induced spin selectivity gives a new twist on spin-control in chemistry," Acc. Chem. Res. **53**, 2659–2667 (2020).

[23] A. G. Volosniev, H. Alpern, Y. Paltiel, O. Millo, M. Lemeshko, and A. Ghazaryan, "Interplay between friction and spin-orbit coupling as a source of spin polarization," Phys. Rev. B **104**, 024430 (2021).

[24] C. Kulkarni, A. K. Mondal, T. K. Das, G. Grinbom, F. Tassinari, M. F. J. Mabesoone, E. W. Meijer, and R. Naaman, "Highly efficient and tunable filtering of electrons' spin by supramolecular chirality of nanofiber-based materials," Adv. Mater. **32**, 1904965 (2020).

[25] C. D. Aiello, J. M. Abendroth, M. Abbas, A. Afanasev, S. Agarwal, A. S. Banerjee, D. N. Beratan, J. N. Belling, B. Berche, A. Botana, J. R. Caram, G. L. Celardo, G. Cuniberti, A. Garcia-Etxarri, A. Dianat, I. Diez-Perez, Y. Guo, R. Gutierrez, C. Herrmann, J. Hihath, S. Kale, P. Kurian, Y.-C. Lai, T. Liu, A. Lopez, E. Medina, V. Mujica, R. Naaman, M. Noormandipour, J. L. Palma, Y. Paltiel, W. Petuskey, J. C. Ribeiro-Silva, J. J. Saenz, E. J. G. Santos, M. Solyanik-Gorgone, V. J. Sorger, D. M. Stemer, J. M. Ugalde, A. Valdes-Curiel, S. Varela, D. H. Waldeck, M. R. Wasielewski, P. S. Weiss, H. Zacharias, and Q. H. Wang, "A chirality-based quantum leap," ACS Nano **16**, 4989–5035 (2022).

[26] F. Evers, A. Aharony, N. Bar-Gill, O. Entin-Wohlman, P. Hedegård, O. Hod, P. Jelinek, G. Kamieniarz, M. Lemeshko, K. Michaeli, V. Mujica, R. Naaman, Y. Paltiel, S. Refaely-Abramson, O. Tal, J. Thijssen, M. Thoss, J. M. van Ruitenbeek, L. Venkataraman, D. H. Waldeck, B. Yan, and L. Kronik, "Theory of chirality induced spin selectivity: Progress and challenges," Adv. Mater. **34**, 2106629 (2022).

[27] S. F. Ozturk, Z. Liu, J. D. Sutherland, and D. D. Sasselov, "Origin of biological homochirality by crystallization of an RNA precursor on a magnetic surface," Sci. Adv. **9**, eadg8274 (2023).

[28] M. R. Wasielewski, "Light-driven spin chemistry for quantum information science," Phys. Today **76**(3), 28–34 (2023).

[29] C. M. Niman, N. Sukenik, T. Dang, J. Nwachukwu, M. A. Thirumurthy, A. K. Jones, R. Naaman, K. Santra, T. K. Das, Y. Paltiel, L. T. Baczewski, and M. Y. El-Naggar, "Bacterial extracellular electron transfer components are spin selective," J. Chem. Phys. **159**, 145101 (2023).

[30] G. Menichetti, L. Cavicchi, L. Lucchesi, F. Taddei, G. Iannaccone, P. Jarillo-Herrero, C. Felser, F. H. L. Koppens, and M. Polini, "Chirality-induced spin polarization in twisted transition metal dichalcogenides," Newton **1**, 100013 (2025).

[31] R. Alhyder, A. Cappellaro, M. Lemeshko, and A. G. Volosniev, "Achiral dipoles on a ferromagnet can affect its magnetization direction," J. Chem. Phys. **159**, 104103 (2023).

[32] K. Banerjee-Ghosh, O. Ben Dor, F. Tassinari, E. Capua, S. Yochelis, A. Capua, S.-H. Yang, S. S. P. Parkin, S. Sarkar, L. Kronik, L. T. Baczewski, R. Naaman, and Y. Paltiel, "Separation of enantiomers by their enantiospecific interaction with achiral magnetic substrates," Science **360**, 1331–1334 (2018).

[33] J. Fransson, "Charge redistribution and spin polarization driven by correlation induced electron exchange in chiral molecules," Nano Lett. **21**, 3026–3032 (2021).

[34] N. Nagaosa, J. Sinova, S. Onoda, A. H. MacDonald, and N. P. Ong, "Anomalous Hall effect," Rev. Mod. Phys. **82**, 1539–1592 (2010).

[35] J. Smit, "The spontaneous Hall effect in ferromagnetics II," Physica **24**, 39–51 (1958).

[36]L. Berger, "Side-jump mechanism for the Hall effect of ferromagnets," Phys. Rev. B **2**, 4559–4566 (1970).
[37]H. Ishizuka and N. Nagaosa, "Spin chirality induced skew scattering and anomalous Hall effect in chiral magnets," Sci. Adv. **4**, eaap9962 (2018).
[38]R. Karplus and J. M. Luttinger, "Hall effect in ferromagnetics," Phys. Rev. **95**, 1154–1160 (1954).
[39]J. M. Luttinger, "Theory of the Hall effect in ferromagnetic substances," Phys. Rev. **112**, 739–751 (1958).
[40]A. Ghazaryan, Y. Paltiel, and M. Lemeshko, "Analytic model of chiral-induced spin selectivity," J. Phys. Chem. C **124**, 11716–11721 (2020).
[41]D. Patterson, M. Schnell, and J. M. Doyle, "Enantiomer-specific detection of chiral molecules via microwave spectroscopy," Nature **497**, 475–477 (2013).
[42]E. I. Rashba, "Spin currents in thermodynamic equilibrium: The challenge of discerning transport currents," Phys. Rev. B **68**, 241315 (2003).
[43]E. I. Rashba, "Spin currents, spin populations, and dielectric function," arXiv:cond-mat/0404723 [cond-mat.mes-hall] (2004).
[44]S. Datta, *Electronic Transport in Mesoscopic Systems*, *Cambridge Studies in Semiconductor Physics and Microelectronic Engineering* (Cambridge University Press, 1995).
[45]B. Gaury, J. Weston, M. Santin, M. Houzet, C. Groth, and X. Waintal, "Numerical simulations of time-resolved quantum electronics," Phys. Rep. **534**, 1–37 (2014), a part of Special Issue: Numerical simulations of time-resolved quantum electronics.
[46]C. W. Groth, M. Wimmer, A. R. Akhmerov, and X. Waintal, "Kwant: A software package for quantum transport," New J. Phys. **16**, 063065 (2014).
[47]T. Kloss, J. Weston, B. Gaury, B. Rossignol, C. Groth, and X. Waintal, "Tkwant: A software package for time-dependent quantum transport," New J. Phys. **23**, 023025 (2021).
[48]M. S. Garelli and J. Schliemann, "Landauer–Büttiker study of the anomalous Hall effect," Phys. Rev. B **80**, 155321 (2009).
[49]D. A. Bahamon, G. Gómez-Santos, D. K. Efetov, and T. Stauber, "Chirality probe of twisted bilayer graphene in the linear transport regime," Nano Lett. **24**, 4478–4484 (2024).
[50]F. J. Lovas, D. f. Plusquellic, B. H. Pate, J. L. Neill, M. T. Muckle, and A. J. Remijan, "Microwave spectrum of 1,2-propanediol," J. Mol. Spectrosc. **257**, 82–93 (2009).
[51]J. Li, L. Hu, and S.-Q. Shen, "Spin-resolved Hall effect driven by spin-orbit coupling," Phys. Rev. B **71**, 241305 (2005).